Fabrication of a facile electrochemical biosensor for Hydrogen peroxide using efficient catalysis of hemoglobin on the porous Pd@Fe_3O_4-MWCNT nanocomposite

Mehdi Baghayeri, Hojat Veisi

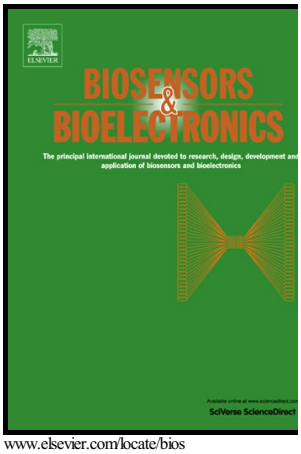

www.elsevier.com/locate/bios

PII: S0956-5663(15)30184-6
DOI: http://dx.doi.org/10.1016/j.bios.2015.06.016
Reference: BIOS7752

To appear in: *Biosensors and Bioelectronic*

Received date: 10 April 2015
Revised date: 22 May 2015
Accepted date: 7 June 2015

Cite this article as: Mehdi Baghayeri and Hojat Veisi, Fabrication of a facile electrochemical biosensor for Hydrogen peroxide using efficient catalysis o hemoglobin on the porous Pd@Fe_3O_4-MWCNT nanocomposite, *Biosensors an Bioelectronic,* http://dx.doi.org/10.1016/j.bios.2015.06.016

Fabrication of a facile electrochemical biosensor for hydrogen peroxide using efficient catalysis of hemoglobin on the porous Pd@Fe_3O_4-MWCNT nanocomposite

Mehdi Baghayeri,[*a] Hojat Veisi[b]

[a]*Department of Chemistry, Faculty of Science, Hakim Sabzevari University, P.O. Box 397, Sabzevar, Iran.*

[b]*Department of Chemistry, Payame Noor University, 19395-4697 Tehran, Iran*

*Corresponding author. Tel: +98 5144013325; fax: +98 5144013170

E-mail address: m.baghayeri@hsu.ac.ir

Abstract

In this work, a sensitive amperometric biosensor for hydrogen peroxide based on synergetic catalysis of hemoglobin and porous Pd@Fe_3O_4-MWCNT nanocomposite has been constructed. With attention to the utilities of large surface area and outstanding catalytic performance, Pd@Fe_3O_4-MWCNT nanocomposite was employed as the nano-stabilizer for the immobilization of hemoglobin (Hb). The immobilized Hb on the surface of nanocomposite as an electrochemical biosensor efficiently catalyzed the reduction of hydrogen peroxide, amplified the electrochemical signal and enhanced the sensitivity. Results of voltammetry and electrochemical impedance examinations showed that the nanocomposite could enhance the electron conductivity and provide more sites for the immobilization of Hb. A linear response from 0.2-500 µM with detection limit of 0.063 µM for hydrogen peroxide was achieved. The apparent Michaelis–Menten constant $K_{app}{}^{M}$ value was 21 µM. Thus, the nanocomposite could be applied for fabrication of a third generation biosensor for hydrogen

peroxide with high sensitivity, selectivity and low detection limit. The excellent performance of the biosensor indicated its promising prospect as a valuable tool in simple and fast hydrogen peroxide detection in environmental and clinical applications.

Keyword: Amperometric biosensor; Hemoglobin; Palladium nanoparticle; Nanocomposite.

1. Introduction

The determination of hydrogen peroxide in biological systems and environment is of tremendous significance due to its effects on the ecosystem and the human health (Ahmed et al., 2012; Wang et al., 2011). Hydrogen peroxide advices as a "substance generally recognized as safe (GRAS)" reagent for food with the mentioned concentration limit value of 80 ppm (Kumar et al., 2012). Owing to the high water solubility of hydrogen peroxide, the aqueous phase chemistry of hydrogen peroxide in the atmosphere is of specific attention. Also, it plays an essential role in a number of main redox processes occurring within the troposphere (Mullaugh et al., 2011). Despite many developments in analytical methods (Campelo et al., 2014; Gimeno et al., 2015; Hu et al., 2014; Lu et al., 2009; Nakamura et al., 2008; Rodrigues et al., 2014), it is still a challenge to find new approaches that could improve the simplicity, selectivity, sensitivity and rapid monitoring for detection of H_2O_2.

Electrochemical biosensors containing enzyme electrodes which catalyze substrate in sequence are mostly used in the determination of H_2O_2 (Mao et al., 2014). Enzyme electrodes consist of two original parts: a conductive part for electroanalytical purposes and a particular enzyme coat that provides the selectivity (Walcarius et al., 2013). The performance of this kind of biosensors greatly depends on the amount of enzyme adsorption, favorable orientations, and suitable interaction of electrode with redox active prosthetic groups of enzymes (Sun et al., 2009). The use of redox mediators between the active redox center of the enzyme and the

electrode surface is very important because the redox center is deeply buried in large three-dimensional protein shells. Considerable efforts have been made to design new applicable biosensors based on use the mediators, promoters, or other special materials to modify the electrode surface (Liu et al., 2013; Charradi et al., 2009; Li et al., 2012; Shao et al., 2011; Li et al., 2008). Among them, metal nanoparticles (NPs) have attracted particular interest owing to their inherent advantages such as electrical conductivity, unique structural and catalytic properties (Mao et al., 2012; Fang et al., 2013). In recent years, noble metal nanoparticles such as gold, platinum and palladium have also attracted much more attention for that they can strongly adsorb some proteins and effectively retain their biological activity (Peng et al., 2013; Sun et al., 2013b; Shervedani and Foroushani, 2014; Zhu et al., 2013; Pan et al., 2012). In most of the cases, these nanoparticles supplied an agreeable microenvironment for the immobilization of enzymes and proteins and enabled the enzyme molecule locate at appropriate orientation, thus facilitated close access of the enzyme to the sensing surface, reduced the insulating property of the enzyme for the direct electron transfer (DET) between the electrode and the immobilized enzyme on the biosensor. However, it is difficult to provide satisfactory support materials to the deposition of noble metal nanoparticles. Many efforts have been developed for the deposition of uniform and small metal NPs on the various solid supports (Wang and Lee, 2007). The ferrimagnetic iron oxide magnetite nanoparticle (Fe_3O_4 NP) can be considered as one of the best interesting materials to be used as a support material. It has the potential for providing the desired magnetic and electrical properties in composite materials. Also, Fe_3O_4 NPs have unique properties such as biocompatibility, super-paramagnetic property, as well as better interaction with desired biomolecules (Rawal et al., 2012; Yang et al., 2014). Preparation of new nanocomposites with favorable interaction of Fe_3O_4 NPs and different noble metal NPs can create unique materials which might open up

new opportunities to investigate the direct electrochemistry of redox enzymes and proteins and fabrication of electrochemical biosensors (Yu et al., 2009).

However, due to their high specific surface areas and magnetic properties, magnetic nanoparticles are often easily self-agglomerated (Teymourian et al., 2013). Therefore, various materials such as SiO_2, carbon nanotubes, and polymers are usually used to immobilize the magnetic nanoparticles and to obtain magnetic nanoparticles with special surface properties that still keep their efficiency. Carbon nanomaterials, such as carbon nanotubes (CNTs) and graphene, are emerging support materials for metal immobilization in analytical applications (Teymourian et al., 2013). Among them, multi walled carbon nanotubes (MWCNTs) could be used an ideal supporter for the immobilization of different nanomaterials through adsorption or suspension crosslinking technique, owing to its low cost, good chemical stability, high surface area, and controllable functionalized process (Bian et al., 2011; Hu et al., 2011). However, the catalyst dispersity on the surface of MWCNT has been considered as a critical factor for the electrocatalytic activity (Chen et al., 2015). In general, it is often not easy to obtain uniform distribution of catalyst particles on a pristine, unmodified MWCNT surface due to inert chemical reactivity. Surface functionalization of pristine MWCNT is usually necessary for introducing binding sites and surface anchoring chemical groups for uniform deposition of catalyst particles. In addition, the surface functionality of the carbon support can exert a unique synergistic effect for final special purpose. Our earlier study showed that covalently functionalized MWCNT with metformin could significantly enhance adhesion of Pd NPs on functionalized MWCNT surface (Baghayeri et al., 2014). The mentioned electrode was used for glucose determination as an enzymatic glucose sensor.

In this report, triethoxyethylcyanide coated magnetic nanoparticles were synthesized by coating triethoxyethylcyanide onto the Fe_3O_4 NPs (Fe_3O_4/Et-CN). Because of the presence of cyanide groups on the Fe_3O_4/Et-CN, Pd nanoparticles could be deposited onto the

magnetic nanoparticles, denoted as Pd@Fe_3O_4. Additionally, by combining the advantageous features of MWCNTs and Pd@Fe_3O_4 NPs, a novel sensing platform has been constructed by integrating MWCNTs with Pd@Fe_3O_4 NPs on a glassy carbon electrode (Pd@Fe_3O_4-MWCNT/GCE). The biosensor is obtained by immobilization of Hb onto Pd@Fe_3O_4-MWCNT nanocomposite modified GC electrode. To the best of our knowledge, there has been no report on the application of noble metallic nanoparticles along with magnetic nanoparticles and MWCNTs for fabrication of a hydrogen peroxide biosensor. Our experimental results revealed that Pd@Fe_3O_4-MWCNT nanocomposite as an excellent nanomaterial could significantly improve the biological activity of the immobilized Hb for reduction of H_2O_2.

2. Experimental

The materials and instrumentation are listed in the Supporting information.

2.1. Synthesis process

2.1.1. Preparation of the Fe_3O_4/Ethyl-CN

Preparation of the magnetic Fe_3O_4 nanoparticles was illustrated in section 1.3 at supporting information. The obtained Fe_3O_4 NPs powder (500 mg) was dispersed in 50 mL toluene solution by sonication for 20 min, and then triethoxyethylcyanide (3 mmol) was added to the mixture. The mixture was refluxed under argon atmosphere at 100 ºC for 48 h. The product was separated by filtration, washed with ethanol, and dried under vacuum for 24 h at 50 ºC. The precipitated product (named Fe_3O_4/Et-CN) was dried at room temperature under vacuum.

2.1.2. Preparation of the Pd@Fe_3O_4 nanoparticles

The Fe_3O_4/Et-CN (500 mg) were dispersed in CH_3CN (30 mL) by ultrasonic bath for 30 min. Subsequently, a yellow solution of $PdCl_2$ (30 mg) in 30 mL acetonitrile was added to dispersion of Fe_3O_4/Et-CN and the mixture was stirred for 10 hours at 20-25 ºC. Then, the Fe_3O_4/Et-CN/Pd(II) was separated by magnetic decantation and washed by CH_3CN, H_2O and acetone respectively to remove the unattached substrates. The Fe_3O_4/Et-CN/Pd(0) nanoparticles were prepared as follows: 50 mg of Fe_3O_4/Et-CN/Pd(II) was dispersed in 60 mL of water, and then 100 μL of hydrazine hydrate (80%) was added. The pH of the mixture was adjusted to 10 with 25% ammonium hydroxide and the reaction was carried out at 95 °C for 2 h. The final product Fe_3O_4/Et-CN/Pd(0) nanoparticles were washed with water, dried in vacuum at 40 °C and named as Pd@Fe_3O_4 nanoparticles. The saturation magnetization value of Pd@Fe_3O_4 nanoparticles was about 55.3 emu g^{-1}, which show a typical super paramagnetic behavior and make them very susceptible to magnetic fields. Scheme 1A depicted the synthetic procedure of Pd@Fe_3O_4 NPs.

2.2. Preparation of modified electrode

Prior to modification, the GCE was polished until a mirror shiny surface appeared, and was sonicated sequentially in acetone, HNO_3 (1:1, v/v), NaOH (1.0 M) and ultra-pure water for 3 min. The Pd@Fe_3O_4-MWCNT nanocomposite was prepared by direct mixing of 0.5 mg MWCNT-NH_2 (amine treatment of MWCNTs was illustrated in section 1.4 at supporting information) and 50 μL Pd@Fe_3O_4 nanoparticles suspension in DMF (2 mg mL^{-1}). The nanocomposite modified GC electrode (Pd@Fe_3O_4-MWCNT/GCE) was fabricated by casting 10 μL of Pd@Fe_3O_4-MWCNT nanocomposite solution onto the surface of GC electrode and drying under room temperature in the air. Afterward, 10.0 μL of 20 mg mL^{-1} Hb solution, dissolved in pH 7.0 PBS, as optimum amount (see Fig. S1 at supporting information) was dropped on the Pd@Fe_3O_4-MWCNT/GCE surface and allowed to dry in

refrigerator at 4 °C for 24 h. Finally, the Hb-immobilized electrode was rinsed throughout with 0.1 M pH 7.0 PBS to wash away the loosely adsorbed Hb molecules. The obtained electrode was labeled as Hb-Pd@Fe_3O_4-MWCNT/GCE. Scheme 1B illustrates the schematic diagram of the Hb biosensor. For comparison, the Hb-MWCNT modified glassy carbon electrode (Hb-MWCNT/GCE) and Hb modified glassy carbon electrode (Hb-GCE) was also prepared according to the same procedure. All the Hb-immobilized electrodes were stored at 4 °C when not in use.

"Here please Scheme 1"

3. Results and Discussion

3.1. Characterization studies on synthesized nanomaterials

The FT-IR spectra of synthesized nanomaterials are characterized in Fig. 1A, which provided direct evidences for the synthetic process. The FT-IR spectrum for the naked magnetic Fe_3O_4 nanoparticles (curve a) shows a stretching vibration at 3381 cm^{-1} which incorporates the contributions from both symmetrical and asymmetrical modes of the O-H bonds which are attached to the surface iron atoms (Luo et al., 2007). The bands at low wave numbers ($\leq$700 cm^{-1}) come from vibrations of Fe-O bonds of iron oxide, in which for the bulk Fe_3O_4 samples appear at 570 and 375 cm^{-1} but for Fe_3O_4 nanoparticles at 624 and 572 cm^{-1} as a blue shift, due to the size reduction (Kassaee et al., 2011; Rao et al., 1995; Waldron, 1955). The presence of an adsorbed water layer is confirmed by a stretch for the vibrational mode of water found at 1622 cm^{-1}. The FT-IR spectra of Fe_3O_4/Et-CN (curve b) and Pd@Fe_3O_4 (curve c) show Fe-O vibrations in the same vicinity. The introduction of cyano groups to the surface of Fe_3O_4 NPs is confirmed by the bands at 1009, 2245 and 2952 cm^{-1} assigned to the Fe-O-Si, CN and C-H stretching vibrations respectively. The cyanide signal appeared at 2245 cm^{-1} in curve b for the metal–ligand co-ordination (Becke, 1996)

presumably leads to a shift of this peak to lower frequency. This shift can be observed comparing curve c. This peak at curves b and c displayed the successful attachment of ethylcyanides organic ligands and subsequent coordination of Pd nanoparticles within the hybrid material.

The X-ray diffraction (XRD) patterns of the Pd@Fe_3O_4 were shown in Fig. 1B. It could be seen that the strong characteristic diffraction peaks at 2θ of 30.09º, 35.44º, 43.07º, 53.43º, 56.96º, and 62.55º corresponding to the diffraction of (220), (311), (400), (422), (511), and (440) of the Fe_3O_4 (JCPDS 89-3854) were found in the sample. This result means that the catalyst have been synthesized successfully without damaging the crystal structure of Fe_3O_4 core. The broad peak at 2θ of 17-25º is assigned to the amorphous silica shell on the surface of the Fe_3O_4 NPs. Moreover, apart from the original peaks, the appearance of the peaks at 2θ of 39.4º, 47.2º, and 67.9º, which corresponding to (111), (200), and (220) crystalline planes of Pd was observed in the spectrum, indicating that Pd^0 exists in the structure of synthesized material.

X-ray photoelectron spectroscopy (XPS) was also carried out to investigate the chemical states of bonded elements in the prepared sample (Fig. 1C). The investigation of the Pd@Fe_3O_4 NPs at the Pd 3p level shows peaks at 532.6 and 553.8 eV for Pd $3p_{3/2}$ and Pd $3p_{1/2}$, respectively, which clearly indicates that the Pd nanoparticles are stable as metallic state in the nanocomposite structure. In comparison to the standard binding energy of Pd^0, with Pd $3p_{3/2}$ of about 532.4 eV and Pd $3p_{1/2}$ of about 560.2 eV (Militello and Simko, 1994), it can be concluded that the Pd peaks in the Pd@Fe_3O_4 shifted to lower binding energy than Pd^0 standard binding energy. It has been reported that the position of Pd 3p peak is usually influenced by the local chemical/physical environment around Pd species besides the formal oxidation state, and shifts to lower binding energy when the charge density around it increases (Teranishi and Miyake, 1998). Therefore, the peaks at 553.8 and 532.6 could be due

to Pd^0 species bound directly to amino groups in the Fe_3O_4/Et-CN, which is in agreement with FT-IR results.

FESEM and TEM were performed to characterize the structure and the morphology of the synthesized Pd@Fe_3O_4 nanoparticles. Fig. 1D shows a representative FESEM image, from which one can observe a uniform nanometer-sized particles with a size range of 5–10 nm. The Pd@Fe_3O_4 nanoparticles were further characterized by taking energy dispersion X-ray spectroscopy (EDS) spectrum, as shown in Fig. S2 (Supporting information). The EDS analysis showed the signals of palladium, iron, silicon and oxygen atoms, which also indicated their presence in the Pd@Fe_3O_4 nanoparticles. Also, the morphology of the Pd@Fe_3O_4 nanoparticles was also investigated by TEM, as shown in Fig. 1E. The images revealed the modified Fe_3O_4 nanoparticles with ethyl cyanide groups as organic shell covered by almost spherical Pd NPs, as shown schematically in inset of Fig. 1E. As shown in Fig. 1E, aggregation of individual NPs was occurred. Such aggregations cause the difference between particle sizes derived from TEM analysis.

"Here please Figure 1"

3.2. Characterization of Pd@Fe_3O_4-MWCNT nanocomposite

Since amino modified MWCNTs (MWCNT-NH_2) are proper supports, Pd@Fe_3O_4 NPs can be attached at their surfaces by appropriate interactions, containing hydrogen bond and electrostatic interactions to fabricate Pd@Fe_3O_4-MWCNT nanocomposite. In order to understand the nature of fabricated nanocomposite, the FT-IR transmittance patterns of MWCNT-NH_2, Pd@Fe_3O_4 and Pd@Fe_3O_4-MWCNT nanocomposite in the frequency range from 4000 to 400 cm^{-1}, are compared in Fig. 2A. Fig. 2A (curve a) shows the FT-IR of the amine treated MWCNT (MWCNT-NH_2). The formation of a peak at 1655 cm^{-1} correspounds to C=O stretching frequency. Also, the peak that corresponds to the C–N stretching vibration

and N–H bending vibration is noted at 1563 cm^{-1} (Tang, 1992; Dong, 1979). The spectral feature of Pd@Fe_3O_4 (curve b) was well demonstrated in previous section. Compared with the spectra of MWCNT-NH_2 and the Pd@Fe_3O_4, it should be noted that the the shift in N-H stretching frequency from 3434 cm^{-1} (curve a) to 3431 cm^{-1} (curve c) with its reduce intensity together confirm the chemically absorbed of Pd@Fe_3O_4 NPs on the surface of MWCNT-NH_2. On the other hand, all vibrations in the two samples are existence in the final composite. These observations confirm the formation of the Pd@Fe_3O_4 NPs on the MWCNT-NH_2.

Furthermore, the SEM image of Pd@Fe_3O_4-MWCNT nanocomposite shows a more uniform surface topography. As shown in Fig. 2B, the homogeneous and dense coverage of Pd@Fe_3O_4 nanoparticles on the MWCNT-NH_2 suggested the successful preparation of Pd@Fe_3O_4-MWCNT nanocomposite. Moreover, nanoparticles remained separate from each other without aggregation, implying the good three-dimensional porous structure of Pd@Fe_3O_4-MWCNT nanocomposite. This three-dimensional porous structure could significantly increase the effective electrode surface and facilitate the immobilization of the proteins onto the film. MWCNTs not only behave as a modifier of Pd@Fe_3O_4 nanoparticles, altering their surface property and preventing their possible agglomeration, but also act as a linkage between Pd@Fe_3O_4 nanoparticles and the electrode surface.

The immobilized Pd nanoparticles on the surface of GCE were probed by cyclic voltammetry. Fig. 2C illustrates the cyclic voltammograms of Pd@Fe_3O_4-MWCNT/GCE in 0.1 M pH 7.0 PBS. The CVs are recorded in the potential range -0.7 to +0.7 V and it clearly shows the presence of Pd on the electrode surface (Rastogi et al., 2014). The Pd@Fe_3O_4-MWCNT/GCE shows separate oxidation/reduction peaks (curve b) which are not observed in MWCNT/GCE (curve a) indicating the existence of Pd NPs. The peak observed at +0.55 V can be attributed to Pd oxide formation and on the reverse scan the peak appeared at -0.01 V is assigned to the reduction of Pd oxide layer formed during the positive scan. The hydrogen

adsorption and desorption peaks are appeared at -0.5 V and -0.4 V respectively (Rastogi et al., 2014).

The structural characteristics of Hb were investigated after it was immobilized on the surface of the nanocomposite. Spectroscopic methods such as FT-IR spectroscopy were used to compare the structural variations of native and immobilized Hb (George and Lee, 2009). The position of the absorption band of Hb in FT-IR spectra can provide information about probable denaturation of Hb. Fig. S3 in supporting information exhibits the FT-IR spectra of Hb and Hb-Pd@Fe_3O_4-MWCNT. Hb-Pd@Fe_3O_4-MWCNT gives absorption bands at 1560 and 1646 cm^{-1} which are the same as the absorption bands at 1560 and 1650 cm^{-1} for native Hb with slight decrease in absorption. Also, the reduced intensity of the IR absorption from 3100-3400 cm^{-1} is observed that might be due to the interaction between Hb and Pd@Fe_3O_4-MWCNT nanocomposite. These results indicate that the secondary structure of Hb immobilized on the surface of Pd@Fe_3O_4-MWCNT nanocomposite is retained the essential features of its native structure. Furthermore, the adsorption ability of Pd@Fe_3O_4-MWCNT nanocomposite for Hb was investigated and the results are shown in supporting information (Fig. S4).

“Here please Figure 2”

3.3. Electrochemical behavior of Hb immobilized on Pd@Fe_3O_4-MWCNT/GCE

The electrochemistry behavior of the Hb immobilized on Pd@Fe_3O_4-MWCNT/GCE is characterized by cyclic voltammetry and electrochemical impedance spectroscopy (EIS). Fig. 3A shows cyclic voltammograms of the Hb-GCE (curve a), Hb-MWCNT/GCE (curve b), Hb-Fe_3O_4-MWCNT/GCE (curve c) and Hb-Pd@Fe_3O_4-MWCNT/GCE (curve d) in 0.1 M PBS, pH 7.0 at scan rate of 0.1 V s^{-1}. The cyclic voltammograms of Hb-MWCNT/GCE, Hb-Fe_3O_4-MWCNT/GCE and Hb-Pd@Fe_3O_4-MWCNT/GCE showed a pair of well-defined

redox peaks with the formal redox potentials (defined as half of sum of anodic and cathodic peak potential, $E^{0'}$) of −0.317 V, −0.312 V and −0.30 V (vs. SCE), respectively, which are close to the $E^{0'}$ value reported previously, attributed to the DET of Hb for the conversion of Hb–heme Fe(III)/Fe(II) redox couple (Shi et al., 2015). However, such redox process is unable to achieve at Hb-GCE under the same condition, suggesting that DET of heme prosthetic group of Hb is awfully difficult at the surface of bare GCE. As it shown, in the absence of Fe_3O_4 nanoparticles, the Hb-MWCNT/GCE (curve b) can also display a couple of redox peaks of Hb. However, the response is 1.8 times smaller than that of the Hb-Fe_3O_4-MWCNT/GCE, indicating that the presence of Fe_3O_4 nanoparticles plays an important role in facilitating the electron exchange between hem centers of Hb and the electrode surface. In fact, the presence of Fe_3O_4 nanoparticles improves the surface area and conductivity of the surface and accelerates the electron transfer between Hb and the electrode surface. On the other hand, Pd NPs are of great interest due to their extensive properties such as large specific surface area, strong adsorption ability and high conductivity. Pd NPs can interact with some biomolecules and act as an inter-mediator to immobilize biomaterials to efficiently retain its activity (Baghayeri et al., 2014). The obtained peak currents from immobilized Hb on the Pd@Fe_3O_4-MWCNT were much larger than those of the Hb-Fe_3O_4-MWCNT/GCE and Hb-MWCNT/GCE, indicating that Pd nanoparticles in the nanocomposite film could increase the adsorption ability for Hb and favor the orientation of Hb. The peak-to-peak separation is 24 mV while the anodic peak current is nearly equal to the cathodic peak current. Therefore, a direct electrochemical reaction is attributed to Hb immobilized on Pd@Fe_3O_4-MWCNT nanocomposite, which indicates that Pd NPs play an important role in promoting the electron transfer between the electroactive center of Hb and electrode surface.

Using Faraday's laws (Zhang et al., 2011), the surface coverage of Hb on the electrode surface was calculated to be 2.72×10^{-10} mol cm^{-2}. This value is much larger than the

theoretical monolayer coverage value (2.86×10^{-12} mol cm^{-2}) of Hb on the bare electrode surface, suggesting that multilayer of Hb participate in the direct electron transfer (Baghayeri et al., 2013). The bigger surface coverage can also be attributed to the present Pd and Fe_3O_4 nanoparticles, as a promising materials for increasing the efficient density of Hb (Zheng et al., 2009), which enables the electric communication with the underlying electrode surface. The buffer pH can strongly affect the electrochemical manners of redox protein on the electrode surface. So the effect of solution pH on the electrochemical response of the Hb-Pd@Fe_3O_4-MWCNT/GCE was investigated and the result presented in Fig. S5 in supporting information. This result confirm that the proton diffusion participate in the electron transfer process of Hb.

The influence of potential scan rate on the electrochemical responses of fabricated biosensor was further investigated by cyclic voltammetry with the results shown in Fig. 3B. The inset a of Fig.3B displays obviously that the anodic (I_{pa}) and cathodic (I_{pc}) peak currents are linearly proportional to the scan rate up to 0.7 Vs^{-1}. This confirms on the one hand that the electroactive species is a surface immobilized one and on the other that in this studied scan rate, a facile electron transfer between surface deposited mediator (Hb in here) and electrode substrate is easily obtainable. Inset b of Fig. 3B illustrates the variation of anodic and cathodic peak potentials, presented as a function of log (scan rate, v). As it can be seen, the separation at anodic and cathodic peak potentials is almost constant for scan rates lower than 0.6 Vs^{-1}, suggesting facile charge transfer kinetics over this range. However, at the higher scan rates, the peak-to-peak separation increased since the charge transfer between immobilized Hb on surface and electrode substrate is affected by kinetic limitations. The charge-transfer coefficient α and the electron transfer rate constant k_s of Hb immobilized on the Pd@Fe_3O_4-MWCNT nanocomposite was calculated to be 0.62 and 2.8 s^{-1} , respectively, by the equations described by Laviron for diffusionless process (Laviron, 1979):

$E_{pc} = E°' - (2.3RT/\alpha nF) \log \upsilon$ (1)

$E_{pa} = E°' - (2.3RT/(1-\alpha)nF) \log \upsilon$ (2)

$\log k_s = \alpha \log(1 - \alpha) + (1 - \alpha) \log \alpha - \log (RT/nF\upsilon) - (1 - \alpha)\alpha F\Delta E_p/2.3RT$ (3)

where n is the number of electron transferred, υ is the scan rate, and $E^{0'}$ is the formal potential and ΔE_p is the peak-to-peak potential separation. R, T and F have their conventional meanings. This calculated k_s value is comparable or higher than that of Hb immobilized on graphene–copper sulfide nanocomposite of 1.58 s^{-1} (Shi et al., 2015), graphene-MWCNT/carbon ionic liquid electrode of 0.97 s^{-1} (Sun et al., 2013a), Hb immobilized on AuNPs-carbon aerogel and ionic liquid of 1.32 s^{-1} (Peng et al., 2015), Hb immobilized on composite film based on ionic liquid and NiO microspheres of 2.54 s^{-1} (Dong et al., 2011) and Hb into halloysite nanotubes/room temperature ionic liquid composite film of 1.51 s^{-1} (Zhang et al., 2012). These results suggested that the Pd@Fe_3O_4-MWCNT nanocomposite facilitates the interfacial electron transfer between Hb heme center and the electrode surface.

The stability of the Hb-Pd@Fe_3O_4-MWCNT/GCE is assessed by using cyclic voltammetry. The peak current and peak potential of the fabricated biosensor over the potential range from -0.5 to -0.1 V have remained nearly unchanged, and the amount of decline after 100 cycles in 0.1 M PBS (pH 7.0) with a scan rate of 0.1 V s^{-1} was less than 1% (Fig. S6, A). On the other hand, the storage stability of the fabricated biosensor was also investigated. When not in use, the biosensor was kept at 4 ◦C in a refrigerator. The results showed that the peak potentials and currents of biosensor were stable for 2 weeks and then decreased slowly. Furthermore, the cyclic voltammetric peak potentials appeared at the same position with the peak current decreased 17% compared with the initial response after 1 month (Fig. S6, B). The excellent stability can be attributed to the promising electrostatic interaction between Hb and Pd@Fe_3O_4-MWCNT nanocomposite. The reproducibility of the fabricated biosensor towards H_2O_2 detection was also studied. The R.S.D. of inter-electrode

responses to 200 μM H_2O_2 at five different electrodes was 7.12% while the R.S.D of intra-electrode responses to five-times repeated additions of 200 μM H_2O_2 was 4.32%.

Furthermore, on the basis of the impedance changes at the electrode surface upon the various modification processes, we infer the successive attachment of Hb on the surface of Pd@Fe_3O_4-MWCNT nanocomposite. The semicircle diameter usually equals to the electron-transfer resistance (R_{et}), which controls the electron-transfer kinetics of the redox probe at the electrode interface/electrolyte interface. Fig. S7 in supporting information explained the typical results of electrochemical impedance spectra of the bare GCE (curve a), MWCNT/GCE (curve b), Pd@Fe_3O_4-MWCNT/GCE (curve c) and Hb-Pd@Fe_3O_4-MWCNT/GCE (curve d), respectively. Obviously, as compared with bare GCE (630 Ω) the whole profile for MWCNT/GCE exhibited a lower diameters (185 Ω) due to the nanotube structure of MWCNT. On the other hand, it was observed that Pd@Fe_3O_4-MWCNT/GCE exhibited an almost straight line (60 Ω), implying that the prepared nanocomposite has excellent electron-transfer advantages and can act similar to electron-conducting tunnels or conducting wires. When Hb immobilized onto Pd@Fe_3O_4-MWCNT/GCE, the electron-transfer resistance for the modified electrode increases greatly (1116.5 Ω). This is caused by the nonconductive property of Hb which acts as an inert electron layer and delayed the electron transfer. In actual, the electrochemical impedance data confirm that the modification of the Pd@Fe_3O_4-MWCNT/GCE with Hb causes a net enhancement in electron-transfer resistance due to the enhanced adsorption protein at the modified electrode surface (Wang et al., 2013).

3.4. Electrocatalysis characteristics of Hb on Pd@Fe_3O_4-MWCNT

Cyclic voltammetry was performed to evaluate the electrocatalytic activity of the immobilized Hb on the nanocomposite for reduction of hydrogen peroxide. From Fig. S8 at

supporting information, when hydrogen peroxide was added to a pH 7.0 PBS, the HbFe(III) reduction peak currents increased obviously accompanied by the decrease of HbFe(II) oxidation peak current, indicating an excellent electrocatalytic activity towards the reduction of hydrogen peroxide. Furthermore, the electrocatalytic performance of Hb at different electrodes was investigated using cyclic voltammetry at presence of hydrogen peroxide and the result presented in Fig. S9 in supporting information. This result obviously confirms that Pd@Fe_3O_4-MWCNT nanocomposite offers a good microenvironment for the fast DET of Hb.

Fig. 3C represents a current–time plot for the biosensor on successive step changes of hydrogen peroxide concentration at the applied potential of -0.4 V vs. SCE. The typical current–time response showed a good analytical performance as presented in Fig. 3C. The time required to reach 95% of the maximum steady-state current is less than 5 s, which indicated a fast process and the Hb could well catalyze the reduction of hydrogen peroxide. The faster response can mainly attribute to the excellent functions of Pd NPs to supply a biocompatible environment for Hb and reduce the distance between the prosthetic groups of Hb and electrode surface. Fig. 3C shows the amperometric current of the biosensor increases with increasing hydrogen peroxide concentration in two concentration ranges. For concentration range 0.2-30 μM (Fig. 3C, inset a), the regression equation was I (μA) = 0.1102 [H_2O_2] μM + 0.1338 μA with correlation coefficient of 0.9956 and detection limit of 0.063 μM based on signal to noise ratio of 3. For higher concentration range of H_2O_2, 30-500 μM (Fig. 3C, inset b), the regression equation was I (μA) = 0.073 [H_2O_2] μM + 0.8272 μA with correlation coefficient of 0.9995. The results offered in Table S1 at supporting information clearly confirm that the various characteristics of the fabricated biosensor are better in some cases or comparable with the other biosensors reported so far. When hydrogen peroxide concentration is at a higher level (more than 500 μM) the response turns from linearity to a platform, demonstrating a characteristic of the Michaelis–Mentien kinetic

mechanism. The apparent Michaelis-Menten constant (K_{app}^{M}), a reflection of the enzyme–substrate kinetics, can be calculated from electrochemical version of the Line weaver–Burk equation (Baghayeri, 2015):

$$(1/I_{ss}) = (1/I_{max}) + (K_{app}^{M}/I_{max}C) \quad (4)$$

where I_{SS} is the steady-state current after the addition of substrate, C is the bulk concentration of the substrate, and I_{max} is the maximum current measured under saturated substrate conditions. K_{app}^{M} value was evaluated to be 21 μM by analysis of the slope and intercept for the plot of the reciprocal of the steady state current versus reciprocal of hydrogen peroxide concentration (inset c of Fig. 3C). The calculated K_{app}^{M} value for the immobilized Hb on Pd@Fe_3O_4-MWCNT nanocomposite is smaller than those of Hb immobilized on carbon nanochips film of 21.55 μM (George and Lee, 2009), Hb in AuNPs-carbon aerogel and ionic liquid film of 0.48 mM (Peng et al., 2015), Hb on graphene-copper sulfide nanocomposite of 6.3 mM (Shi et al., 2015) and Hb at a network of crosslinked carbon nanotube on a thiol-modified Au Surface of 0.19 mM (Kafi and Crossley, 2013). This result offers again that the biosensor maintains higher biological affinity to hydrogen peroxide and the Hb on the nanocomposite retained its biocatalytic activity. The selectivity of the biosensor towards hydrogen peroxide also investigated by amperometric method (Fig. S10) and the results were presented at supporting information.

"Here please Figure 3"

As mentioned at introduction section, hydrogen peroxide is a chemically oxidant which plays a main role in a number of important redox processes occurring within environment (Mullaugh et al., 2011). Also, it is the result of oxidative stress and metabolism and play significant role in clinical analysis. Therefore, in order to prove the reliability of the proposed biosensor for hydrogen peroxide detection, we applied the modified electrode to the

determination of hydrogen peroxide in spiked rain water (as environment sample) and urine (as clinical sample) samples. The urine samples obtained from a local laboratory under optimum conditions without any sample pretreatment other than a dilution step with PBS (pH 7.0). The determined results were compared with those obtained by using the classical potassium permanganate titration method. The obtained results are shown in Table 1. The results are in good agreement with each other, indicating the potential practical application of our proposed biosensor for hydrogen peroxide in real samples.

"Here please Table 1"

4. Conclusion

Herein, we have proposed an amperometric biosensor for hydrogen peroxide based on the synergistic catalysis of hemoglobin and Pd@Fe_3O_4-MWCNT nanocomposite immobilized on GCE. With the advantages of large surface area, good conductivity and excellent catalytic performance, Pd@Fe_3O_4-MWCNT nanocomposites could act such as conducting wires and largely enhanced the immobilized amount of the Hb, paving the way for direct electron transfer between the Hb protein and the electrode surface. Moreover, the presented studies show very good direct electrochemical characteristics and performances of Hb at fabricated biosensor for determination of hydrogen peroxide with high sensitivity, good reproducibility and very low detection limit. In this way, the developed biosensor could be also successfully applied for analyzing two different types of real sample analysis.

Acknowledgment

We would like to thank the Hakim Sabzevari University for its financial support.

References

Ahmed, W., Sidhu, J.P.S., Toze, S., 2012. Environ. Sci. Technol. 46, 6843-6850.

Baghayeri, M., 2015. RSC Adv. 5, 18267-18274.

Baghayeri, M., Nazarzadeh, E.N., Namadchian, M., 2013. Sens. Actuators, B 188, 227-234.

Baghayeri, M., Veisi, H., Veisi, H., Maleki, B., Karimi-Maleh, H., 2014. RSC Adv. 4, 49595-49604.

Becke, A.D., 1996. J. Chem. Phys. 104, 1040-1046.

Bian, C.-L., Zeng, Q.-X., Yang, L.-J., Xiong, H.-Y., Zhang, X.-H., Wang, S.-F., 2011. Sens. Actuators, B 156, 615-620.

Campelo, G., Souza, S.D., Bezerra, P.A., Paula, A., Paim, S., Marques, D., Paim, A.P.S., Lavorante, A.F., 2014. Food Control. 46, 127-135.

Charradi, K., Forano, C., Prevot, V., Ben Haj Amara, A., Mousty, C., 2009. Langmuir 25, 10376-10383.

Chen, C., Lin, C., Chen, L., 2015. Electrochim. Acta 152, 408-416.

Dong, Q.N., 1979. IR Spectrum Method, Publishing house of the Chemical Industry, Beijing.

Dong, S., Zhang, P., Liu, H., Li, N., Huang, T., 2011. Biosens. Bioelectron. 26, 4082-4087.

Fang, Y., Wang, E., 2013. Chem. Commun. 49, 9526-9539.

George, S., Lee, H.K., 2009. J. Phys. Chem. B 113, 15445-15554.

Gimeno, P., Bousquet, C., Lassu, N., Civade, C., Brenier, C., Lempereur, L., 2015. J. Pharm. Biomed. Anal. 107, 386-393.

Hu, A., Liu, Y., Deng, H., Hong, G., Liu, A., 2014. Biosens. Bioelectron. 61, 374-378.

Hu, Y., Li, J., Zhang, Z., Zhang, H., Luo, L., Yao, S., 2011. Anal. Chim. Acta 698, 61-68.

Kafi, A.K.M., Crossley, M.J., 2013. Biosens. Bioelectron. 42, 273-279.

Kassaee, M.Z., Masrouri, H., Movahed, F., 2011. Appl. Catal. A: Gen. 395, 28-33.

Kumar, S., Palani, B., Pillai, K.C., 2012. Colloids Surf., A 395, 207-216.

Laviron, E., 1979. J. Electroanal. Chem. 101, 19-28.

Li, J., Tang, J., Zhou, L., Han, X., Liu, H., 2012. Bioelectrochemistry 86, 60-66.

Li, Y., Zeng, X., Liu, X., Liu, X., Wei, W., Luo, S., 2010. Colloids Surf., B 79, 241-245.

Liu, Q., Yu, J., Xu, Y., Wang, J., Ying, L., Song, X., Zhou, G., Chen, J., 2013. Electrochim. Acta 92, 153-160.

Lu, S., Song, J., Campbell-palmer, L., 2009. Sci. Hortic. 120, 336-341.

Luo, S., Zheng, X., Xu, H., Mi, X., Zhang, L., Cheng, J.-P., 2007. Adv. Synth. Catal. 349, 2431-2434.

Mao, C.-J., Chen, X.-B., Niu, H.-L., Song, J.-M., Zhang, S.-Y., Cui, R.-J., 2012. Biosens. Bioelectron. 31, 544-547.

Mao, X., Rutledge, G.C., Hatton, T.A., 2014. Nano Today 9, 405-432.

Militello, M.C., Simko, S.J., 1994. Surf. Sci. Spectra 3, 387-392.

Mullaugh, K.M., Kieber, R.J., Willey, J.D., Avery, G.B., 2011. Environ. Sci. Technol. 45, 9538-9542.

Nakamura, H., Mogi, Y., Akimoto, T., Naemura, K., Kato, T., Yano, K., Karube, I., 2008. Biosens. Bioelectron. 24, 455-460.

Pan, Z.-Q., Shi, C.-G., Fan, H., Bao, N., Yu, C.-M., Liu, Y., Lu, R., Zhang, Q.-H., Gu, H.-Y., 2012. Sens. Actuators, B 174, 421-426.

Peng, H., Liang, R., Zhang, L., Qiu, J., 2013. J. Electroanal. Chem. 700, 70-76.

Peng, L., Dong, S., Li, N., Suo, G., Huang, T., 2015. Sens. Actuators, B 210, 418-424.

Rao, Z.M., Wu, T.H., Peng, S.Y., 1995. Acta Phys. Chim. Sin. 11, 395-399.

Rastogi, P.K., Ganesan, V., Krishnamoorthi, S., 2014. Electrochim. Acta 125, 593-600.

Rawal, R., Chawla, S., Devender, Pundir, C.S., 2012. Enzyme Microb. Technol. 51, 179-185.

Rodrigues, S.S.M., Ribeiro, D.S.M., Molina-garcia, L., Medina, A.R., Prior, J.A.V., Santos, J.L.M., 2014. Talanta 122, 157-165.

Shao, Q., Wu, P., Gu, P., Xu, X., Zhang, H., Cai, C., 2011. J. Phys. Chem. B 115, 8627-8637.

Shervedani, R.K., Foroushani, M.S., 2014. Bioelectrochemistry 98, 53-63.

Shi, F., Zheng, W., Wang, W., Hou, F., Lei, B., Sun, Z., Sun, W., 2015. Biosens. Bioelectron. 64, 131-137.

Sun, W., Cao, L., Deng, Y., Gong, S., Shi, F., Li, G., Sun, Z., 2013a. Anal. Chim. Acta 781, 41-47.

Sun, W., Li, L., Lei, B., Li, T., Ju, X., Wang, X., et al., 2013b. Mater. Sci. Eng., C 33, 1907-1913.

Sun, W., Li, X., Wang, Y., Li, X., Zhao, C., Jiao, K., 2009. Bioelectrochemistry 75, 170-175.

Tang, H.T., 1992. Organic Compound Spectra Determination, Publishing house of Beijing University, Beijing

Teranishi, T., Miyake, M., 1998. Chem. Mater. 10, 594-600.

Teymourian, H., Salimi, A., Khezrian, S., 2013. Biosens. Bioelectron. 49, 1-8.

Walcarius, A., Minteer, S.D., Wang, J., Lin, Y., Merkoçi, A., 2013. J. Mater. Chem. B 1, 4878-4908.

Waldron, R.D., 1955. Phys. Rev. 99, 1727-1735.

Wang, Y., Lee, J., 2007. J. Mol. Catal. A: Chem. 263, 163-168.

Wang, Y.-H., Yu, C.-M., Pan, Z.-Q., Wang, Y.-F., Guo, J.-W., Gu, H.-Y., 2013. Microchim. Acta 180, 659-667.

Wang, Z., Liu, F., Teng, X., Zhao, C., Lu, C., 2011. Analyst 136, 4986-4990.

Yang, Z., Zhang, C., Zhang, J., Bai, W., 2014. Biosens. Bioelectron. 51, 268-273.

Yu, C.-M., Guo, J.-W., Gu, H.-Y., 2009. Microchim. Acta 166, 215-220.

Zhang, H., Meng, Z., Wang, Q., Zheng, J., 2011. Sens. Actuators, B 158, 23-27.

Zhang, Y., Cao, H., Fei, W., Cui, D., Jia, N., 2012. Sens. Actuators, B 162, 143-148.

Zheng, N., Zhou, X., Yang, W., Li, X., Yuan, Z., 2009. Talanta 79, 780-786.

Zhu, L., Xu, L., Tan, L., Tan, H., Yang, S., Yao, S., 2013. Talanta 106, 192-199.

Figure and scheme captions

Scheme 1. (A) Representation route for preparation of Pd@Fe_3O_4 nanocomposite. (B) Schematic illustration for the direct electron transfer from Hb to GCE at fabricated biosensor.

Fig. 1. (A) FT-IR spectra of naked magnetic Fe_3O_4 nanoparticles (curve a), Fe_3O_4/Et-CN (curve b) and Pd@Fe_3O_4 (curve c). (B) XRD patterns of the Pd@Fe_3O_4 NPs. (C) X-ray photoelectron spectroscopy of the Pd@Fe_3O_4 NPs. (D) SEM images of Pd@Fe_3O_4 NPs. (E) Typical TEM image of Pd@Fe_3O_4 NPs.

Fig. 2. (A) FT-IR spectra of MWCNT-NH_2 (curve a), Pd@Fe_3O_4 NPs (curve b) and Pd@Fe_3O_4-MWCNT nanocomposite (curve c). (B) SEM image of Pd@Fe_3O_4-MWCNT nanocomposite. (C) CVs of MWCNT/GCE (curve a) and Pd@Fe_3O_4-MWCNT/GCE (curve b) in 0.1 M pH 7.0 PBS.

Fig. 3 (A) Cyclic voltammograms of the Hb-GCE (a), Hb-MWCNT/GCE (b), Hb-Fe_3O_4-MWCNT/GCE (c) and Hb-Pd@Fe_3O_4-MWCNT/GCE (d) in N_2-saturated 0.1 M pH 7.0 PBS at scan rate of 0.1 V s^{-1}. (B) Cyclic voltammograms of Hb-Pd@Fe_3O_4-MWCNT/GCE in 0.1

M PBS (pH 7.0) at different scan rates of (1) 0.02, (2) 0.04, (3) 0.06, (4) 0.08, (5) 0.1, (6) 0.15, (7) 0.2, (8) 0.3, (9) 0.4, (10) 0.5, (11) 0.6 and (12) 0.7 V s^{-1}. Inset a: Plot of the anodic (1) and cathodic (2) peak current against the scan rate. Inset b: Relationship of the anodic (1) and cathodic (2) peak potential against log υ. (C) Amperometric response of the biosensor to successive addition of different concentration of hydrogen peroxide in 0.1 M PBS (pH 7.0) at the working potential of -0.4 V. Inset a: plot of electrocatalytic peak current vs. concentration of hydrogen peroxide (0.2-30 μM). Inset b: plot of electrocatalytic peak current vs. concentration of hydrogen peroxide (30-500 μM). Inset c: plot of the reciprocal of steady-state current (I_{ss}) versus the reciprocal of hydrogen peroxide concentration for the Hb-Pd@Fe_3O_4-MWCNT/GCE.

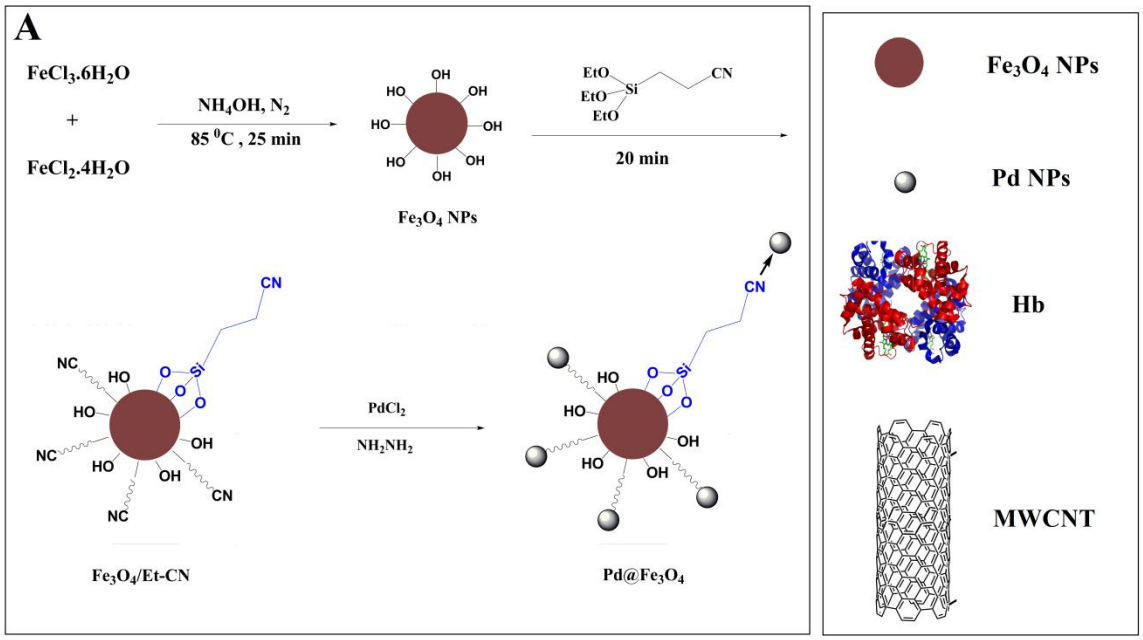
A
FeCl3.6H2O
+
FeCl2.4H2O
NH4OH, N2
85 0C , 25 min
Fe3O4 NPs
20 min
PdCl2
NH2NH2
Fe3O4/Et-CN
Pd@Fe3O4
Fe3O4 NPs
Pd NPs
Hb
MWCNT

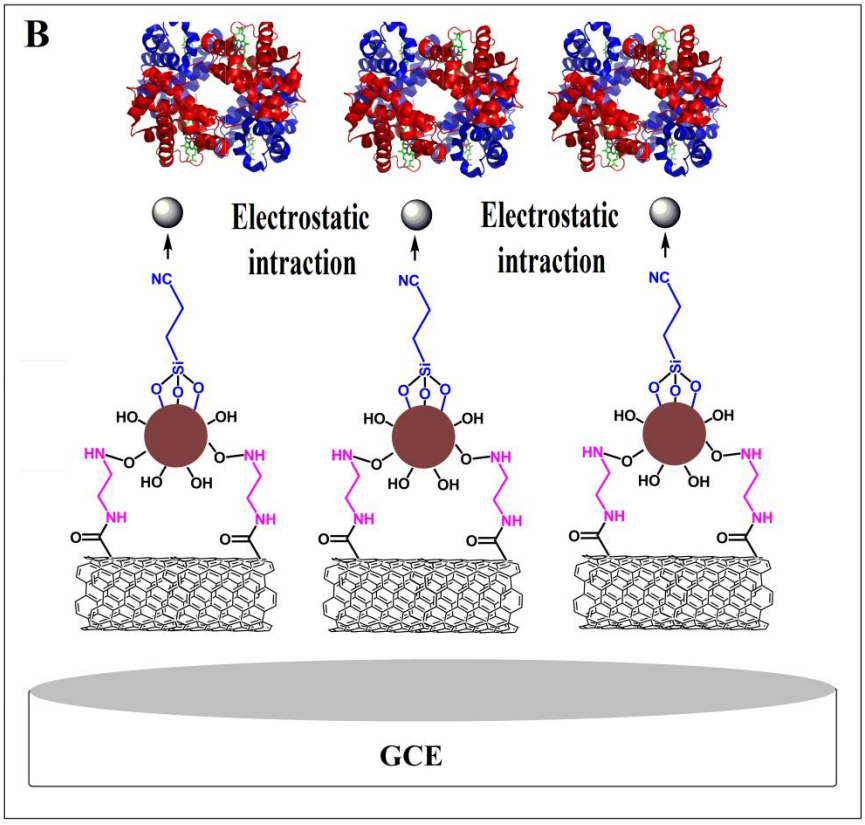
B
Electrostatic intraction
Electrostatic intraction
GCE

Scheme 1

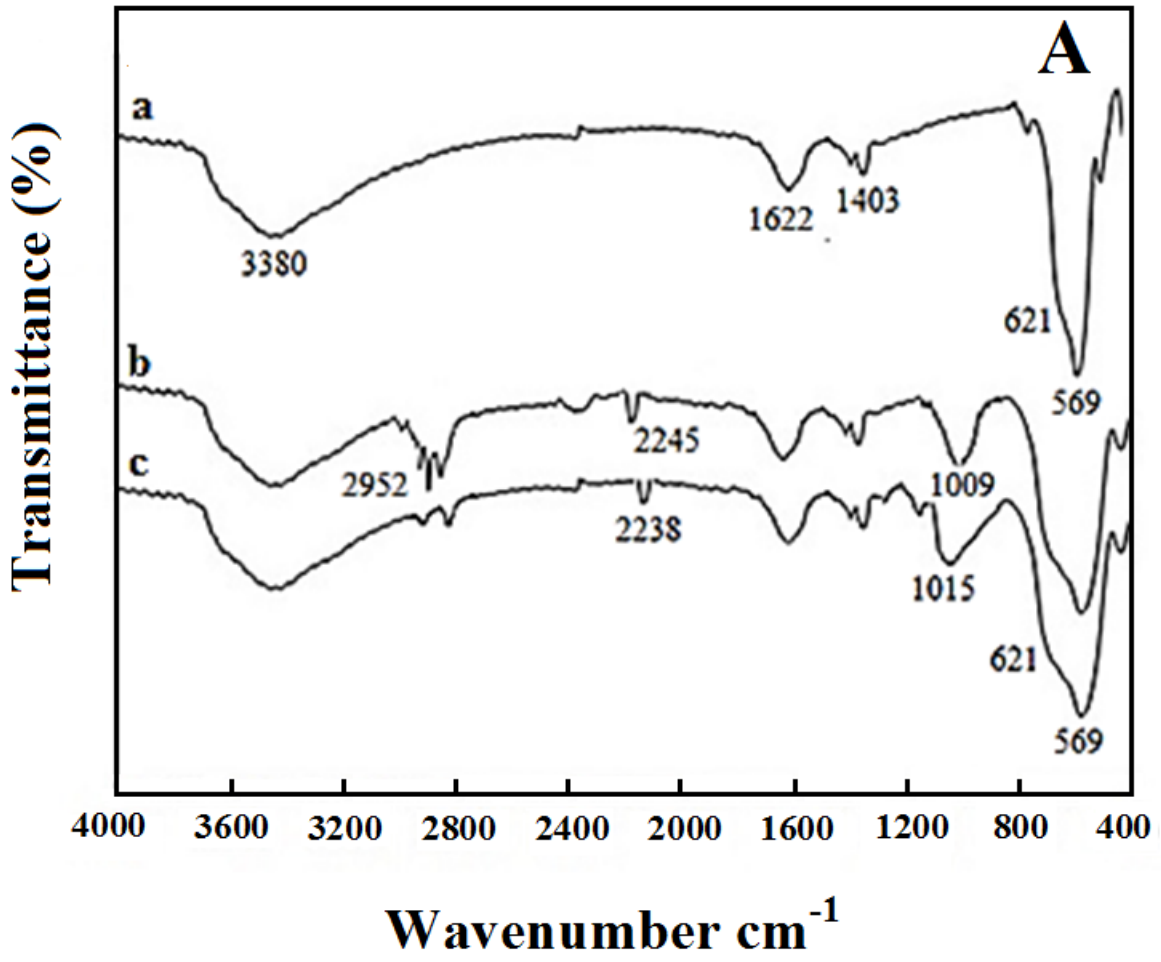

Figure 1A

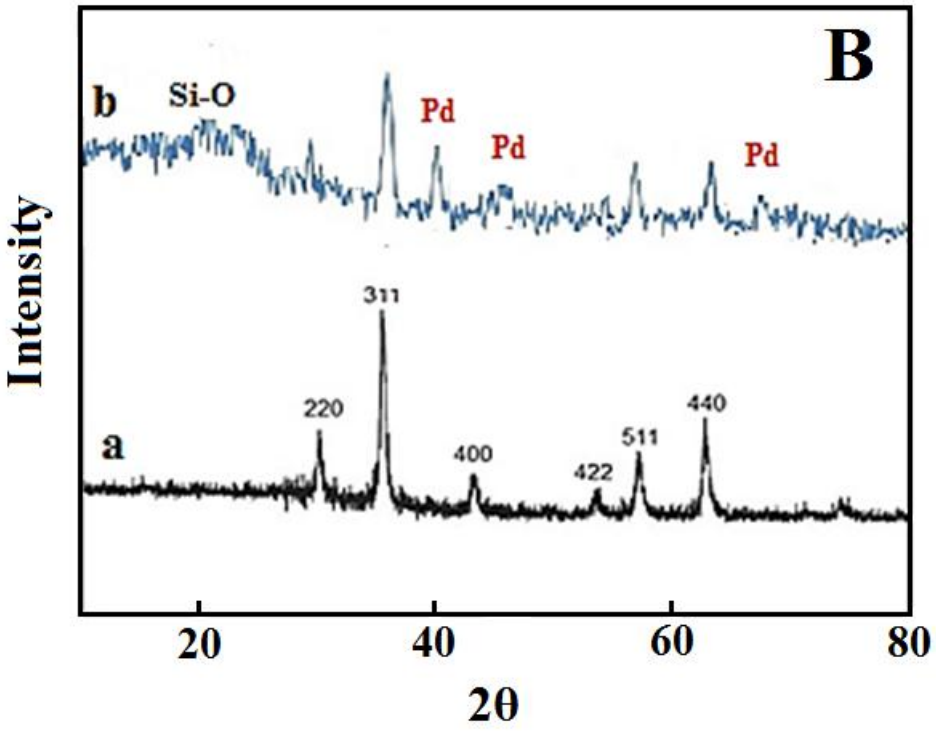

Figure 1B

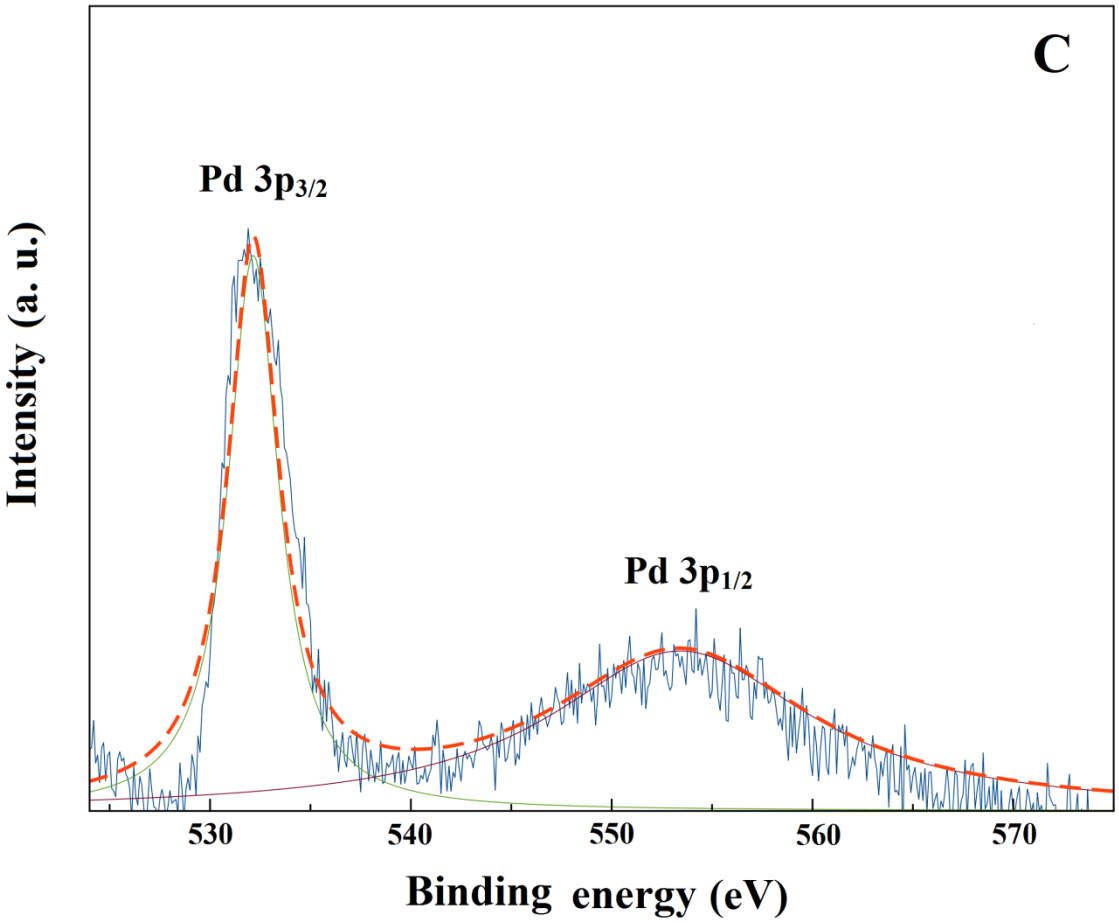

Figure 1C

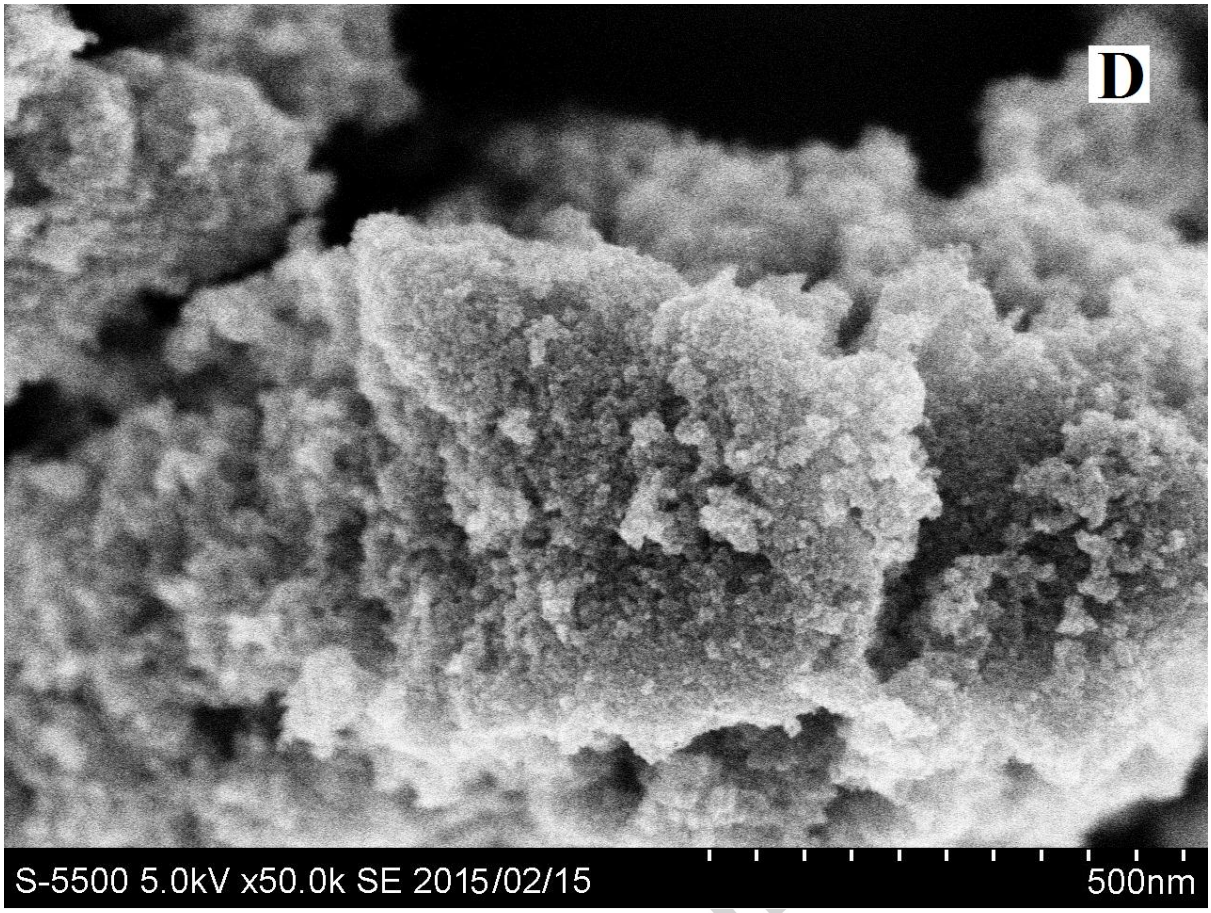

Figure 1D

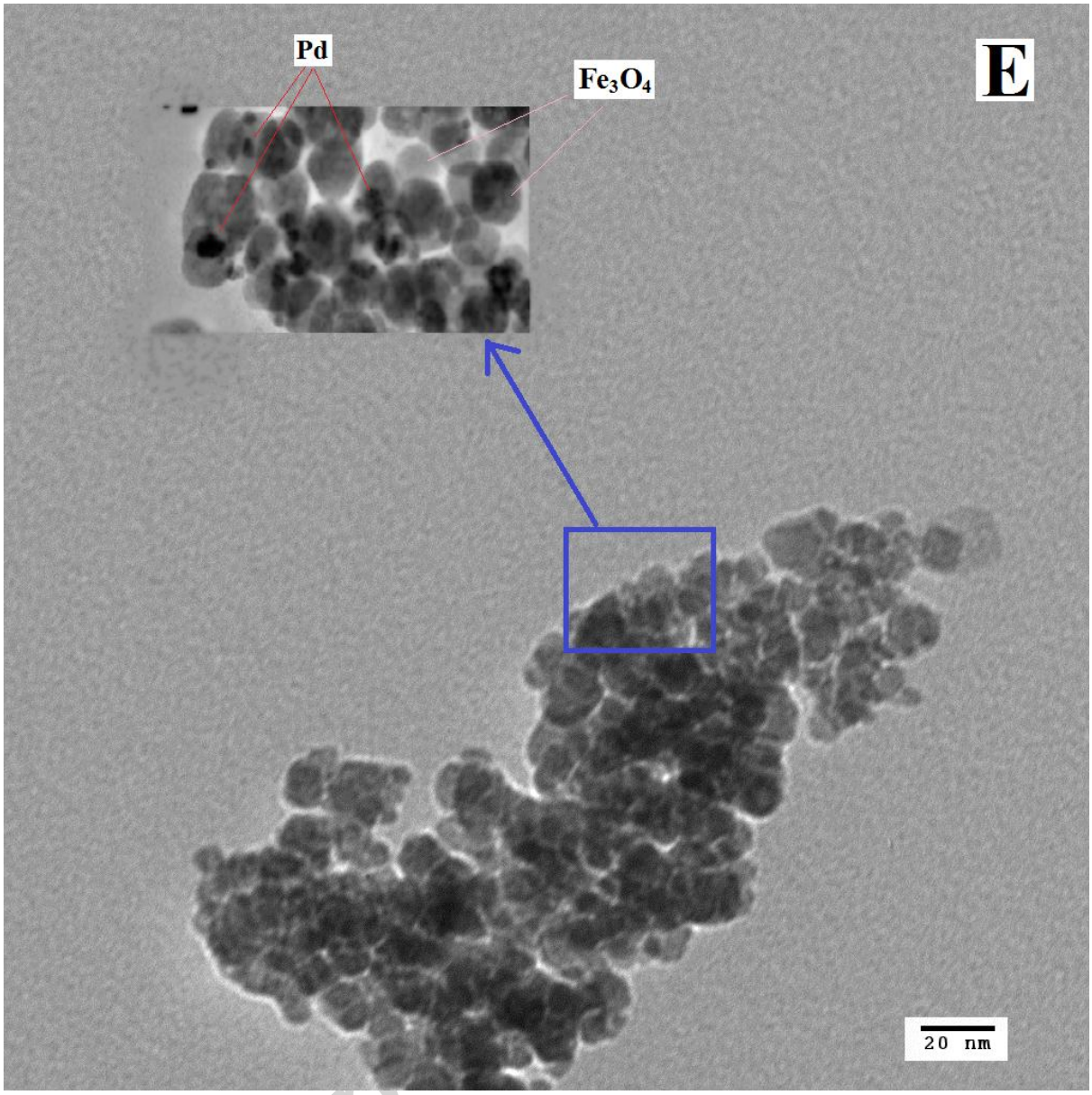

Figure 1E

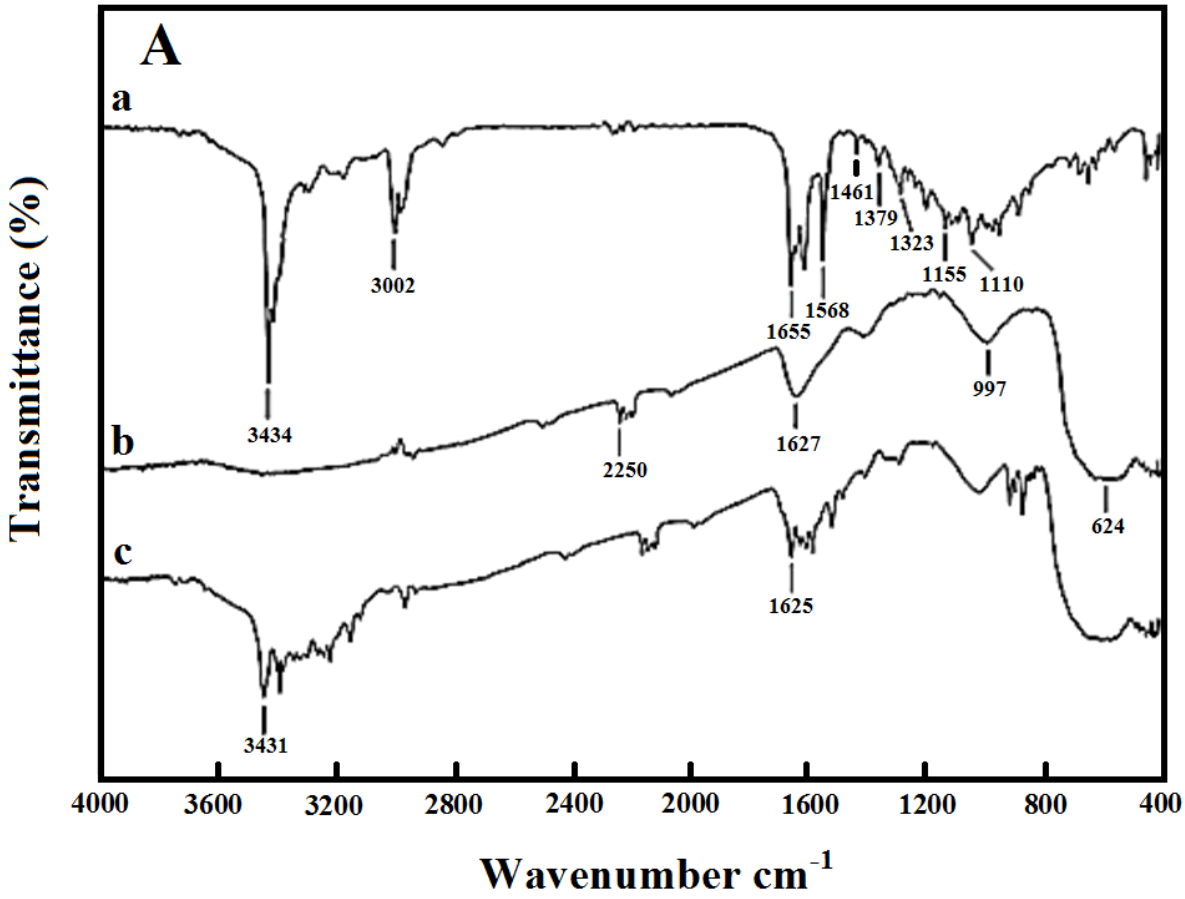

Figure 2A

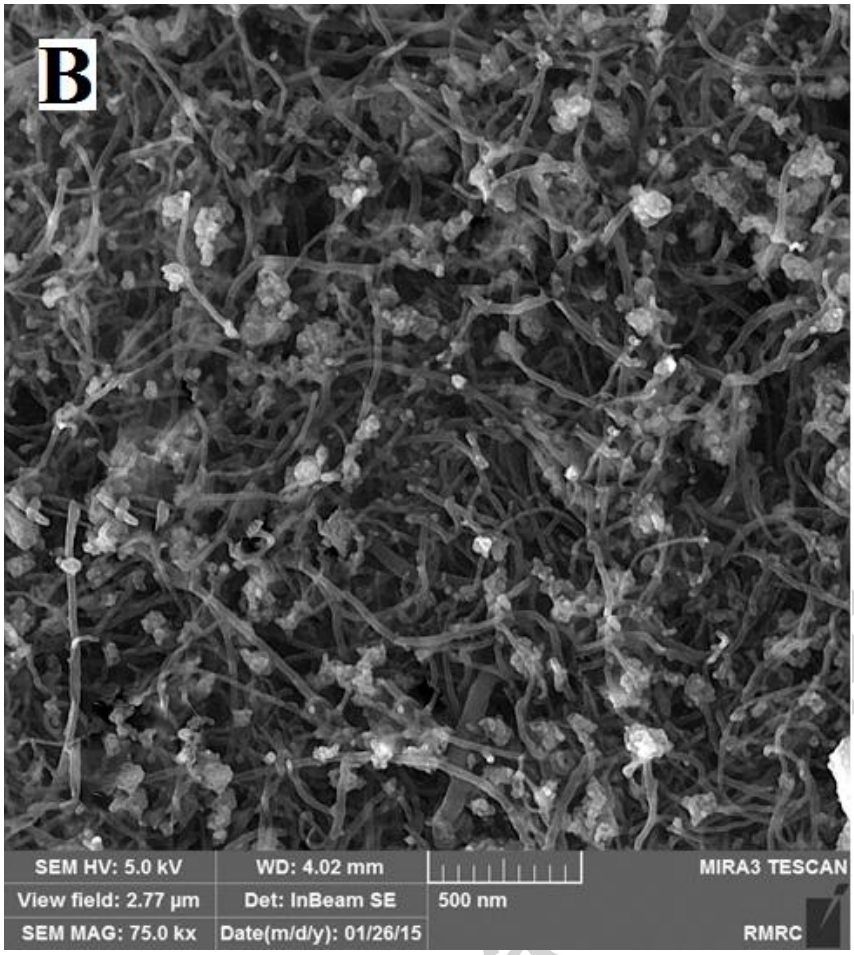

Figure 2B

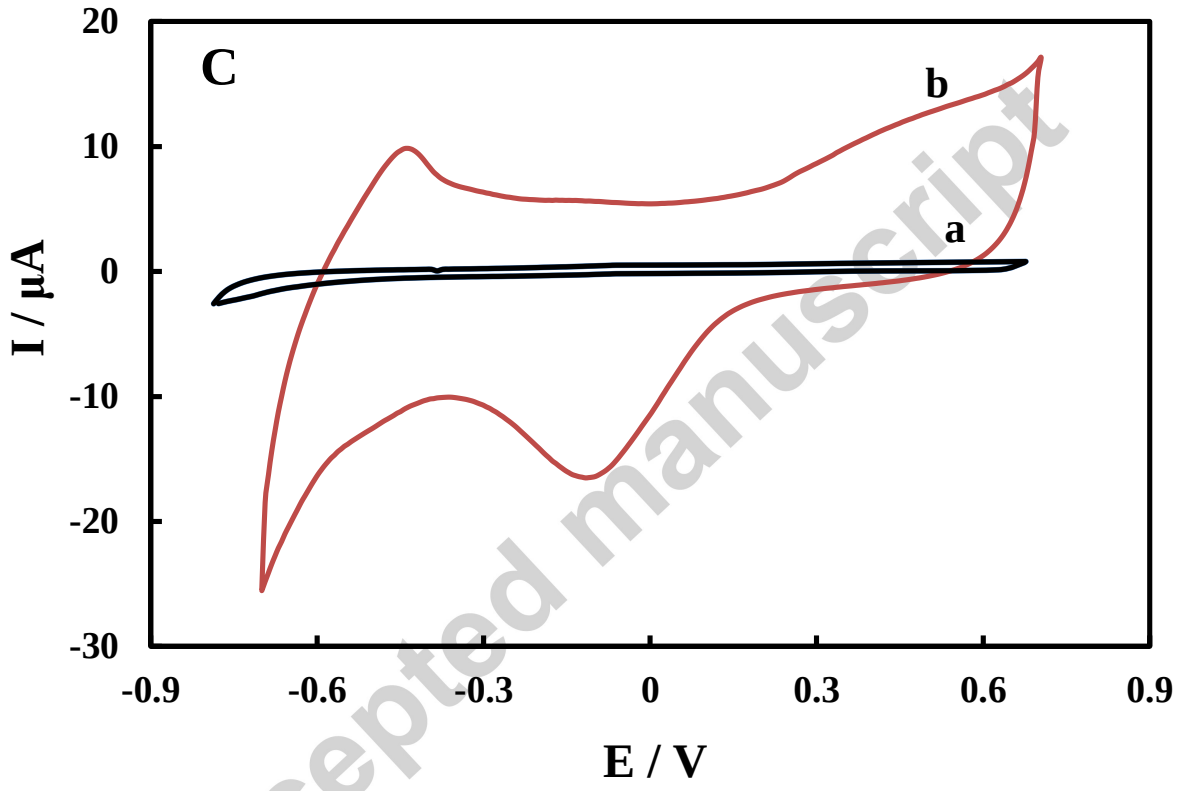

Figure 2C

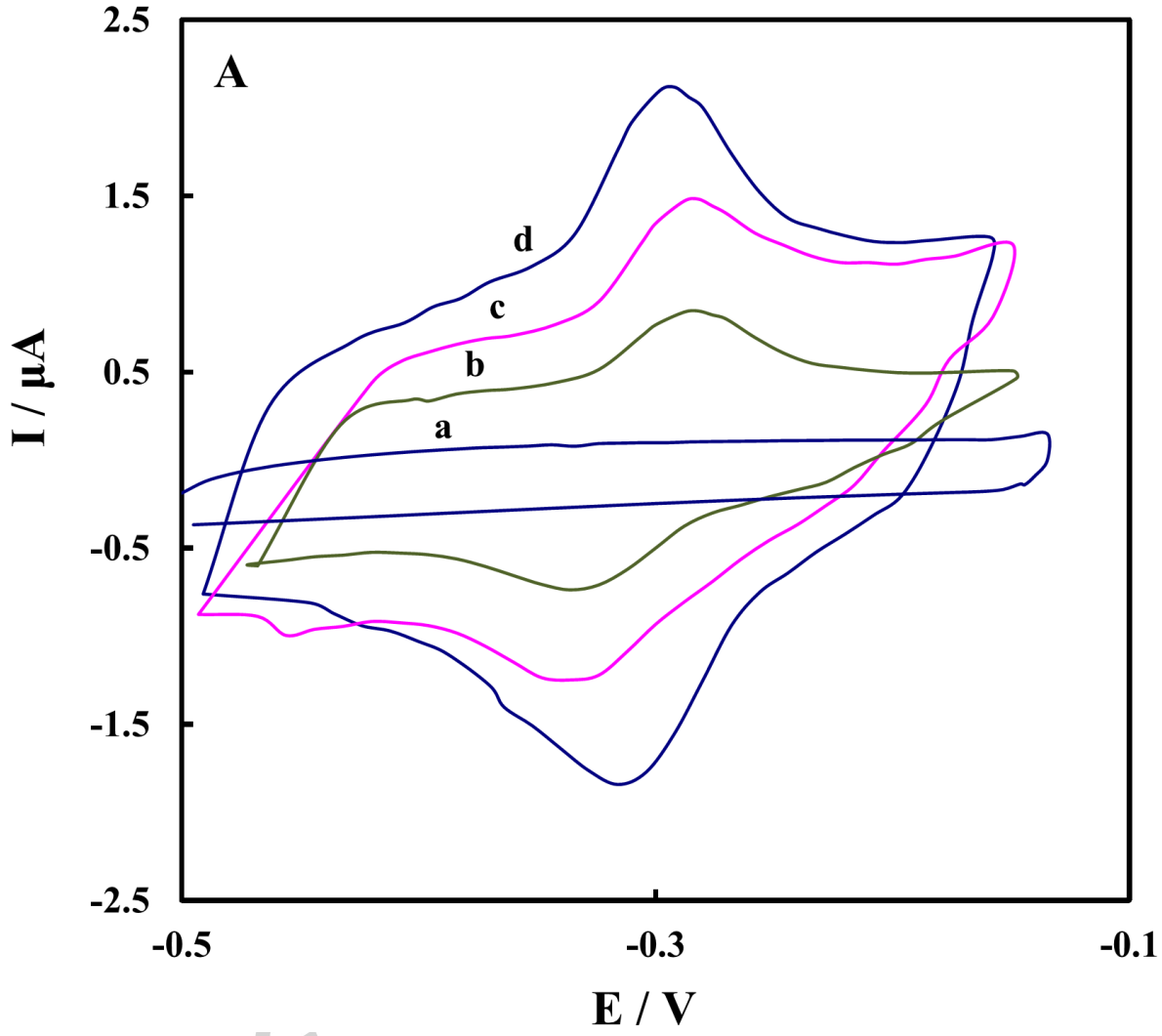

Figure 3A

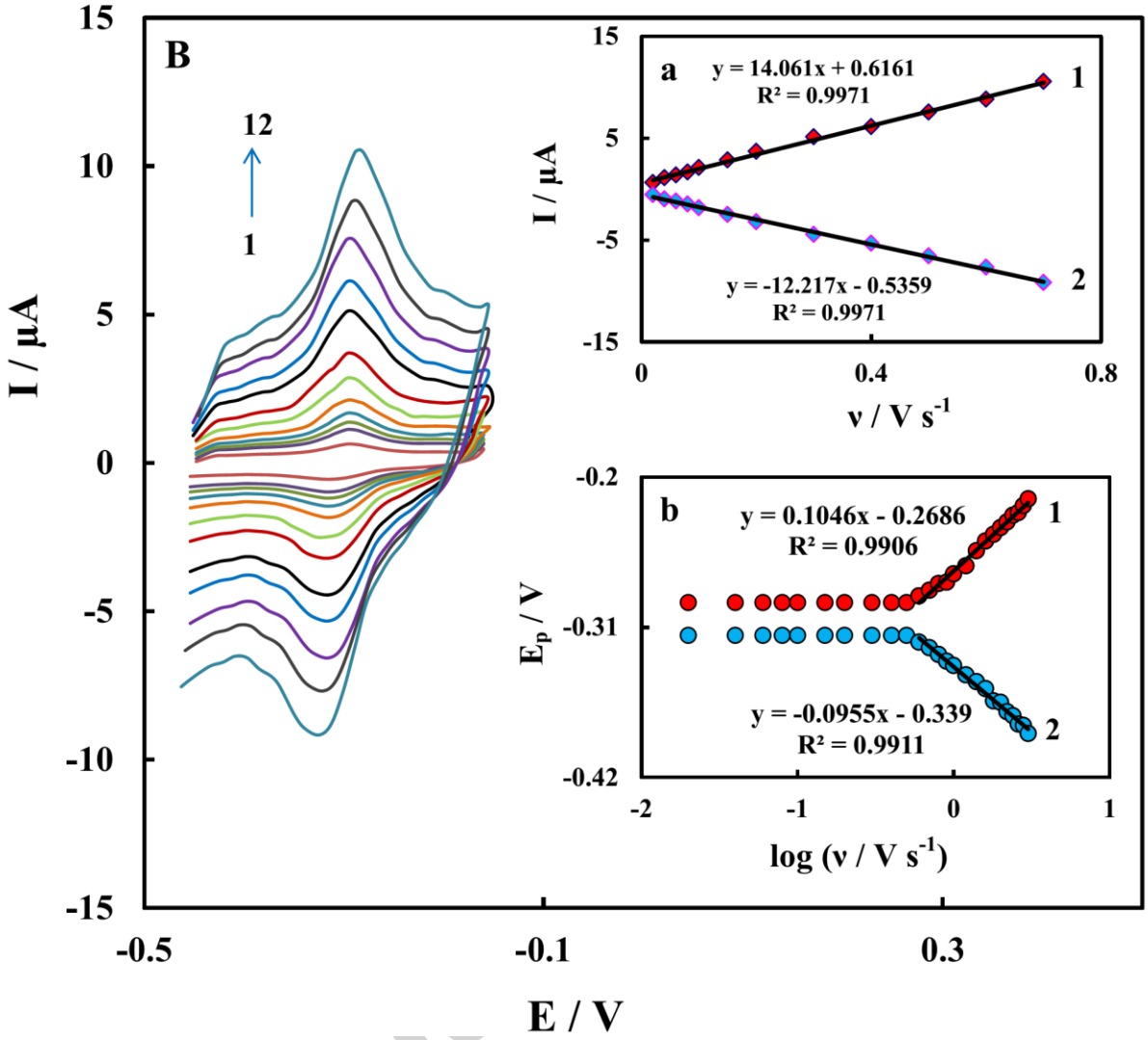

Figure 3B

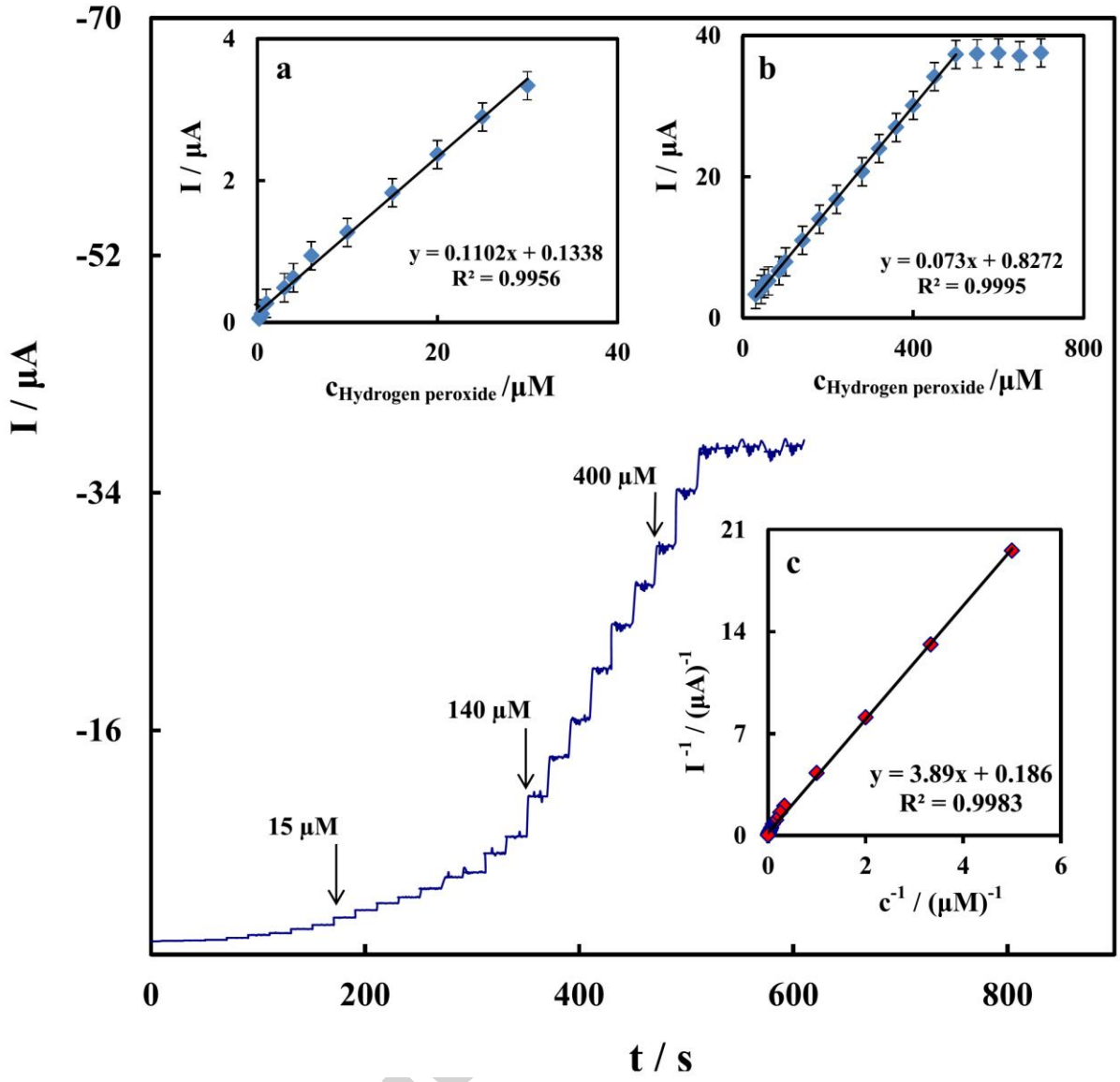

Figure 3C

Table 1

Results of the hydrogen peroxide detection and the recovery test for real sample analysis (n=5).

Sample	Added (μM)	Found (μM)	R.S.D	Recovery (%)	Determined by titration method	R.S.D
A	0	168±0.06	1.9	-	167.2	1.2
	30	197±0.06	1.8	99.4	-	-
	50	217.4±0.03	2.2	99.7	-	-
B	0	183±0.04	2.3	-	182.3	2.1
	80	261.6±0.05	1.6	99.4	-	-
	120	302.4±0.07	3.3	99.8	-	-
C	0	-	-	-	-	-
	10	10.5±0.06	3.2	105	10.2	2.1
	50	50.9±0.04	2.2	101.8	50.4	1.7
D	0	-		-	-	
	100	99.8±0.05	1.8	99.8	101.2	1.2
	200	200.2±0.06	2.1	100.1	200.6	2.3

A and B samples of hydrogen peroxide in urine samples.

C and D samples of hydrogen peroxide in rain samples.

Highlights

● A novel electrochemical platform based on Pd@Fe_3O_4-MWCNT nanocomposite was proposed and used for biosensor fabrication.

● The nanocomposite exhibited an excellent ability towards the immobilization of Hb.

● The presented Hb-based biosensor showed high analytical performance of for detection of hydrogen peroxide.

● The proposed biosensor showed high sensitivity and sub-micro molar detection limits.